Supporting Information

# Metal organic framework derived hierarchical copper cobalt sulfide nanosheet arrays for high-performance solid-state asymmetric supercapacitors

Ahmed Bahaa [1], Jayaraman Balamurugan[1], Nam Hoon Kim [1*], Joong Hee Lee [1, 2*]

[1]Advanced Materials Institute of BIN Convergence (BK plus Global) & Department of BIN Convergence Technology, Chonbuk National University
[2]Center for Carbon Composite Materials, Department of Polymer & Nano Science and Technology, Chonbuk National University, Jeonju, Jeonbuk, 54896, Republic of Korea

[*]Corresponding to Prof. Nam Hoon Kim (nhk@chonbuk.ac.kr)
Prof. Joong Hee Lee (jhl@chonbuk.ac.kr)

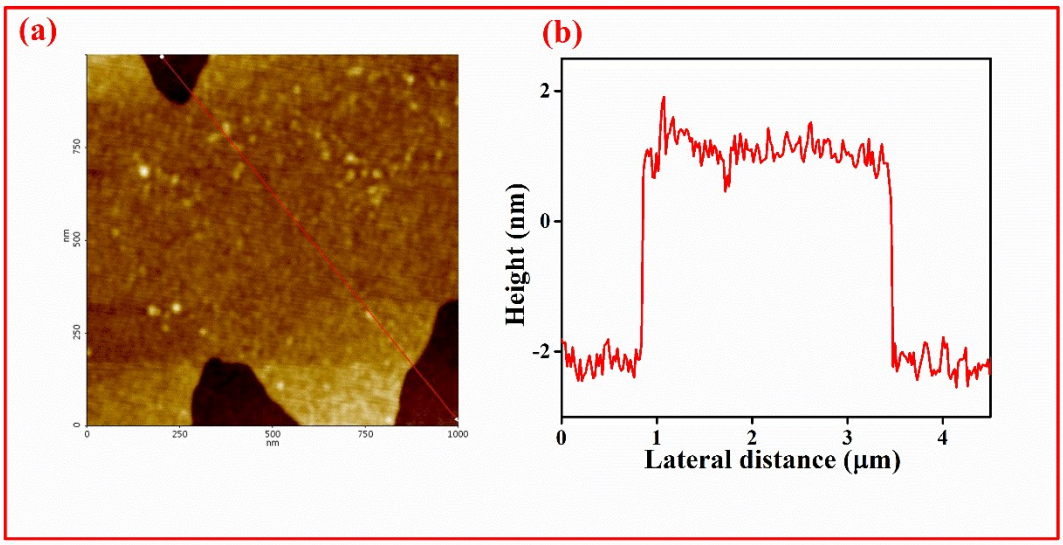


**Fig. S1** a, b 2D AFM image and its height profile of $CuCo_2S_4$ NS arrays, representing thickness around 2 nm.

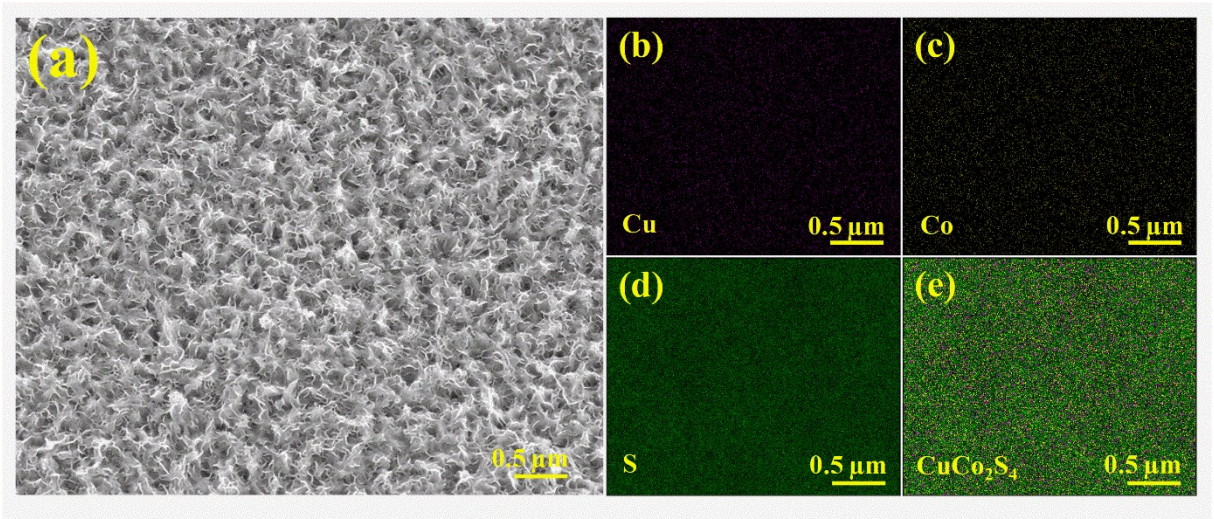


**Fig. S2** a–e SEM image of $CuCo_2S_4$ NS arrays and its corresponding SEM-EDS color mapping with respect to Cu-K, Co-K and S-K.

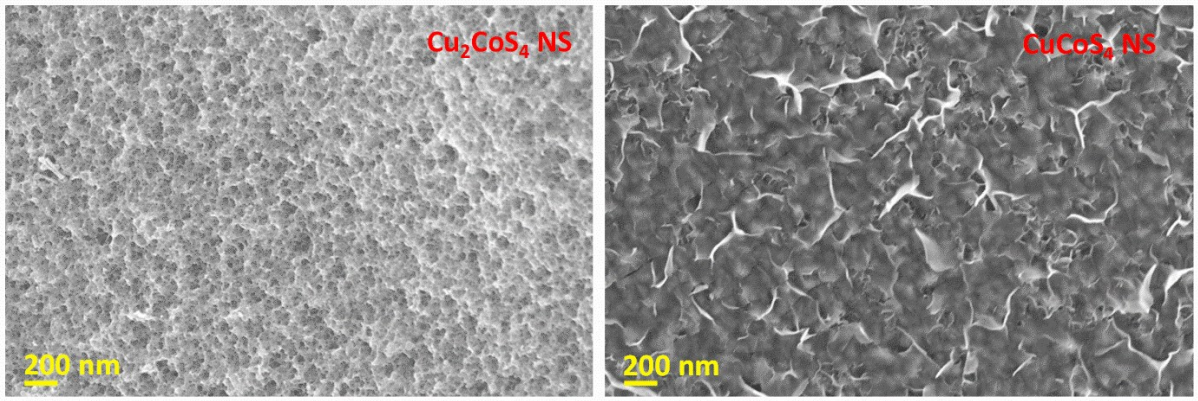


**Fig. S3** SEM images of $Cu_2CoS_4$ and $CuCoS_4$ NS arrays.

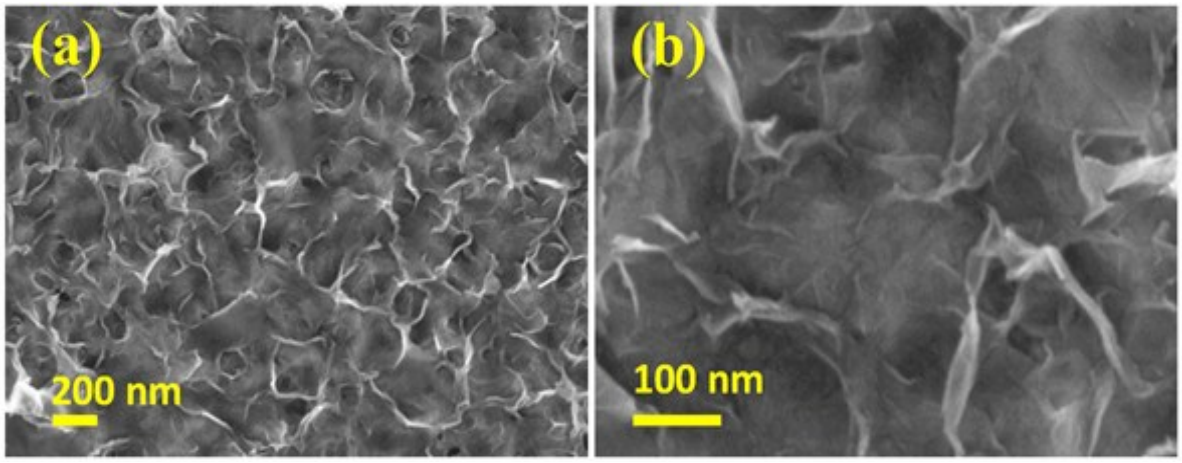


**Fig. S4** a and b. SEM images at different magnification of $CuCo_2S_4$ NS-U.

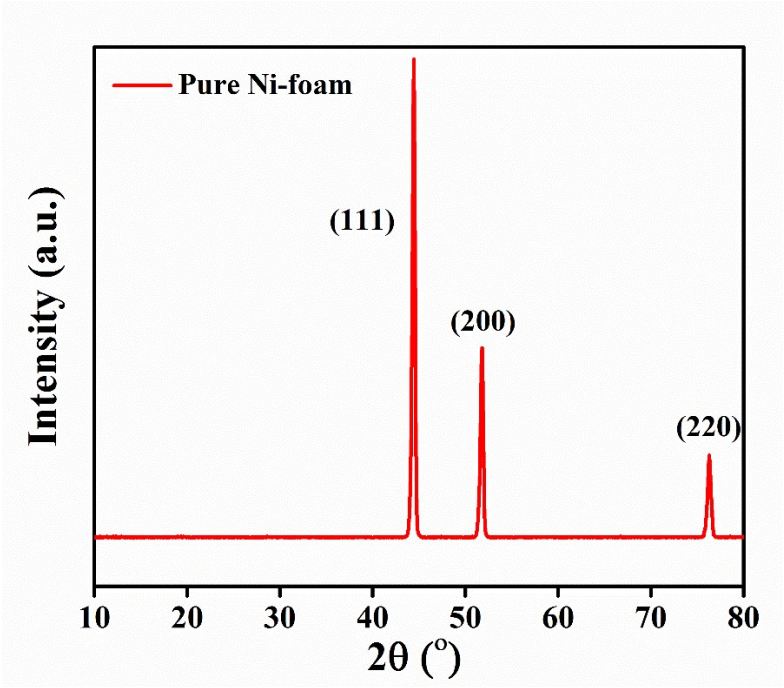


**Fig. S5** XRD pattern of pure Ni foam.

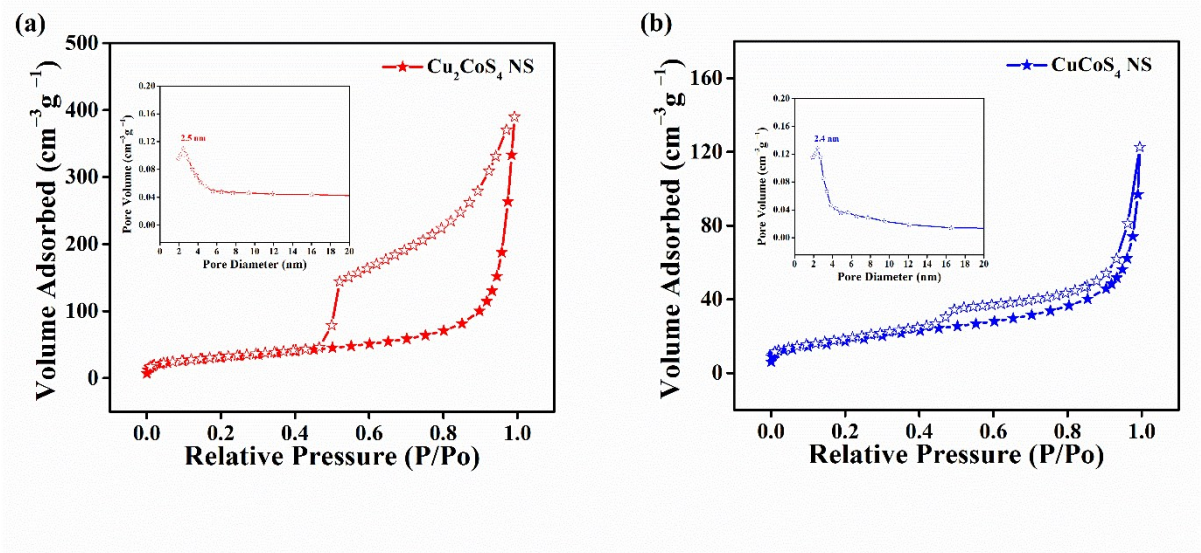


**Fig. S6** $N_2$ sorption isotherms of (a) $Cu_2CoS_4$ and (b) $CuCoS_4$ NS arrays (inset shows their corresponding pore size distribution curves).

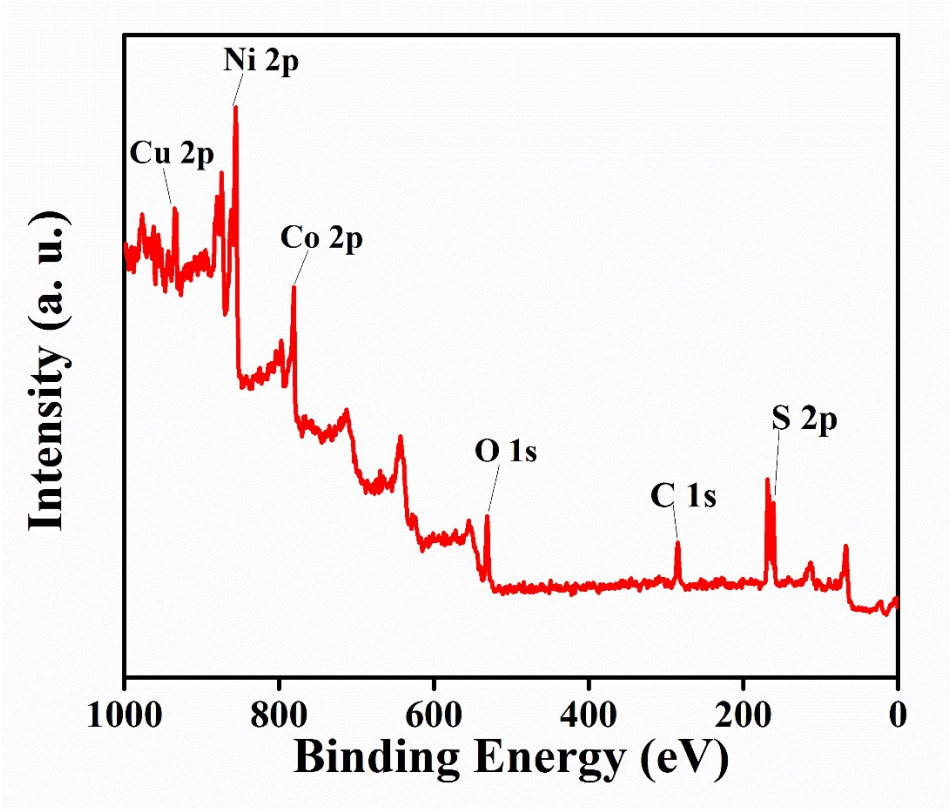


**Fig. S7** XPS survey spectrum of $CuCo_2S_4$ NS arrays.

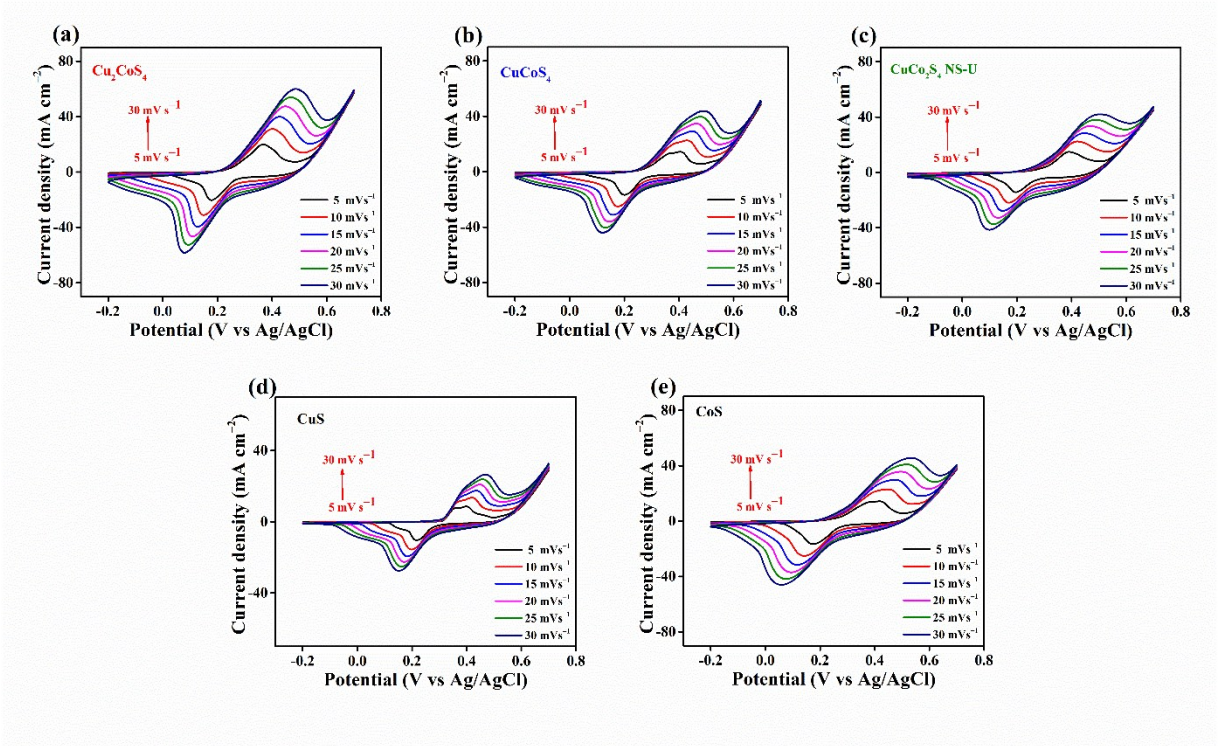


**Fig. S8** (a-e) CV curves of $Cu_2CoS_4$ NS, $CuCoS_4$ NS, $CuCo_2S_4$ NS-U, CuS, and CoS electrodes with different scan rates from 5to 30 mV $s^{-1}$.

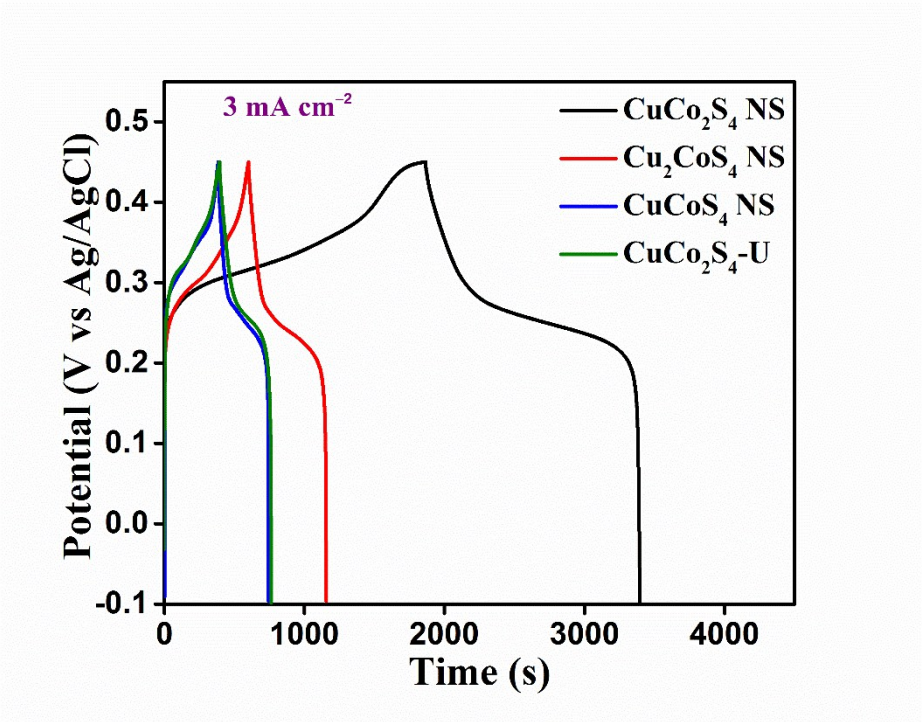


**Fig. S9** GCD curves of $CuCo_2S_4$ NS, $Cu_2CoS_4$ NS, $CuCoS_4$ NS, and $CuCo_2S_4$ NS-U electrodes at a current density of 3 mA cm$^{-2}$.

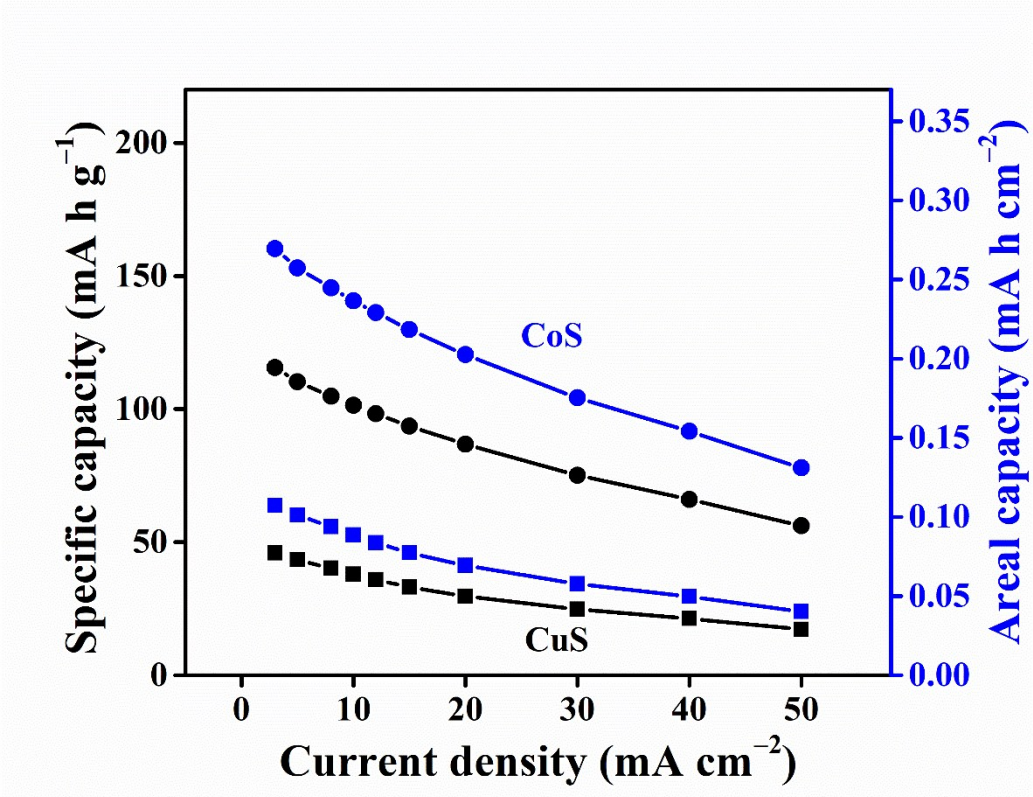


**Fig. S10** Specific and areal capacity of CuS and CoS electrodes as a function of current density.

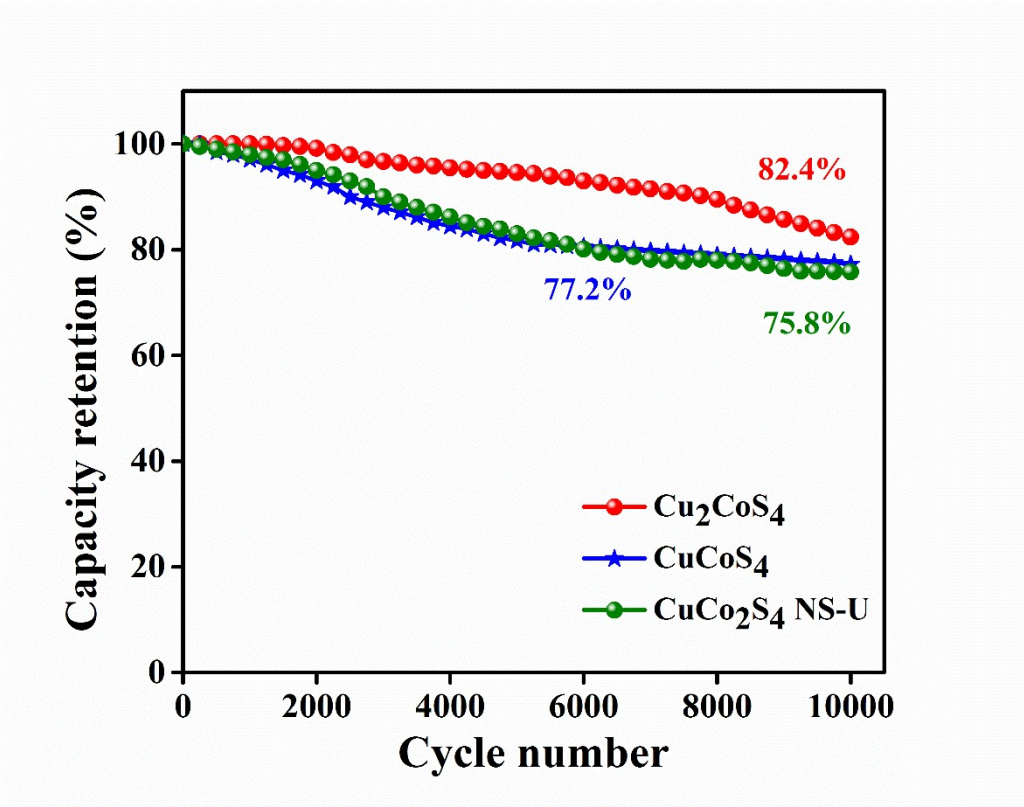


**Fig. S11** Cyclic performance of $Cu_2CoS_4$ NS, and $CuCoS_4$ NS, and $CuCo_2S_4$ NS-U electrodes at a current density of 30 mA $cm^{-2}$.

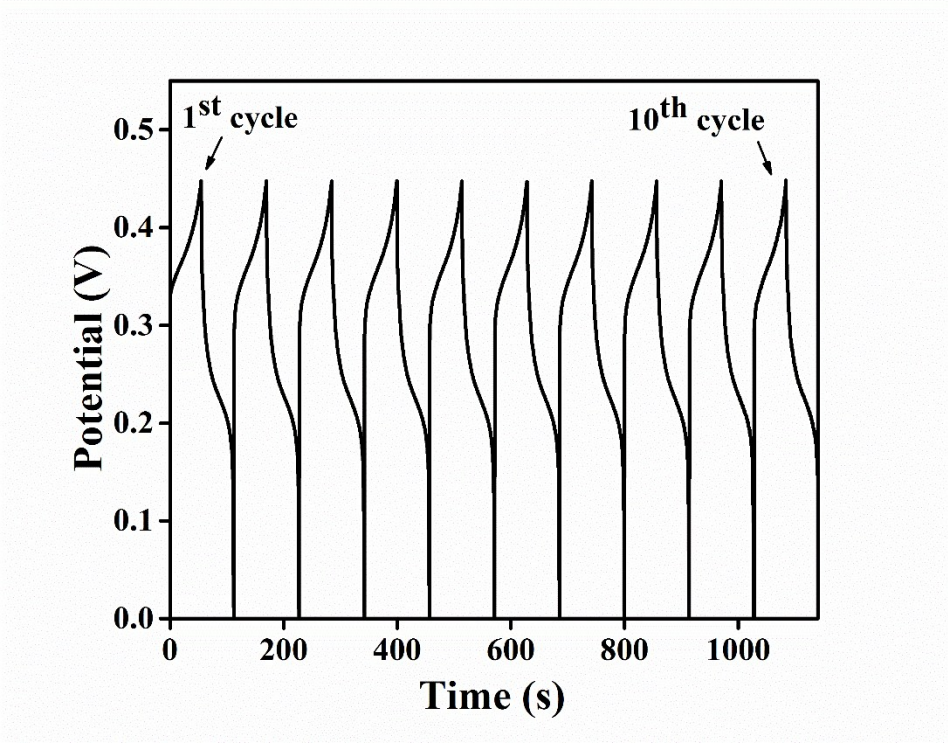


**Fig. S12** The first ten cycles of the fabricated $CuCo_2S_4$ NS arrays at a current density of 30 mA $cm^{-2}$.

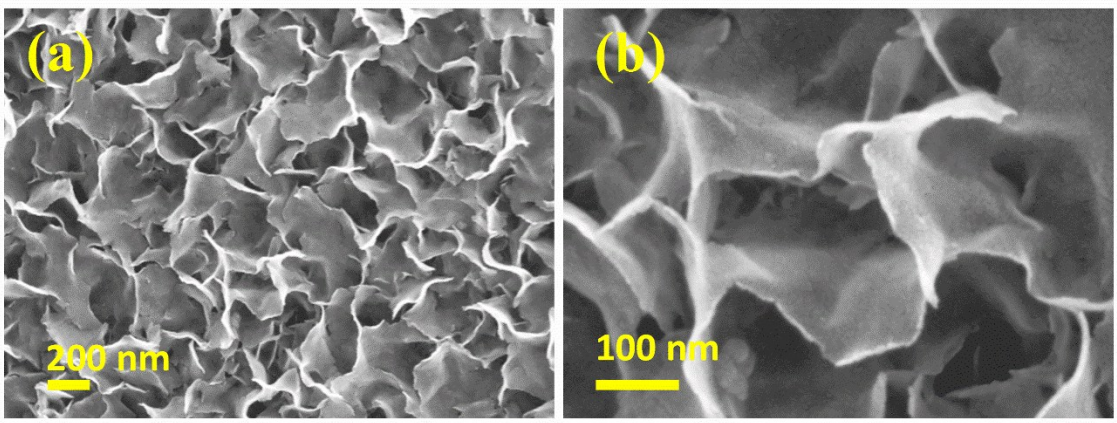


**Fig. S13** SEM images at different magnifications of $CuCo_2S_4$ NS arrays (after 10000 charge-discharge cycling test).

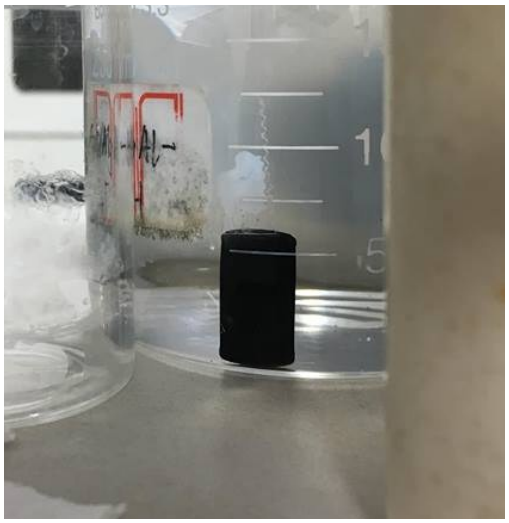

**Fig. S14** Digital photograph of $Fe_2O_3$/NG hydrogel with a perfect cylinderical shape.

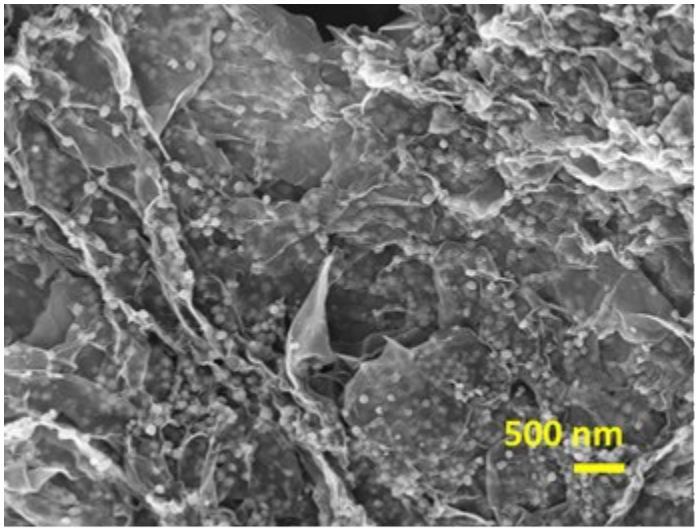


**Fig. S15** SEM image of $Fe_2O_3$/NG aerogel.

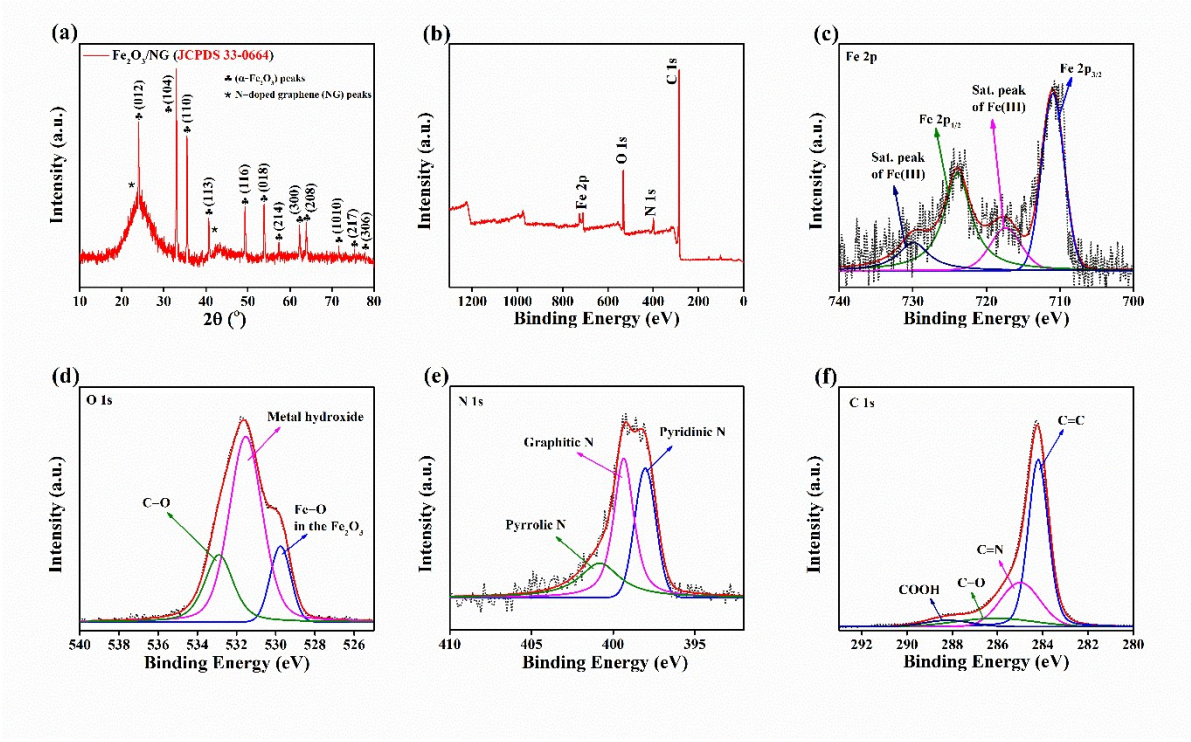


**Fig. S16** (a) XRD of the $Fe_2O_3$/NG aerogel, (b) XPS survey spectrum of $Fe_2O_3$/NG aerogel, High-reolution XPS spectra of (c) Fe 2p, (d) O 1s, (e) N 1s, and (f) C 1s for the $Fe_2O_3$/NG aerogel.

The high-resolution Fe 2p spectrum (Fig. S16c) displays the Fe $2p_{3/2}$ centered at ~710.9 eV, and Fe $2p_{1/2}$ centered at ~724.4 eV. In addition, the shake-up satellite peaks at ~717.3 eV, ~730.9 eV represent Fe (III) ions in the $Fe_2O_3$ (Fig. S16c).[1] The O peak around 532 eV can be split into three peaks at (529.9 eV) which present the oxygen in the $Fe_2O_3$, (532.2 eV), and (533.3 eV) represent the existence of oxygen in the metal hydroxide and carbon bond, respectively (Fig. S16d).[2] The N 1s peak can be fitted to three components based on different binding energies: for pyridinic (398.1 eV), graphitic (399.2 eV), and pyrrolic (400.8 eV) Fig. S16e. Among the three nitrogen bonding formations, pyridinic N and graphitic N have been shown to result in highly active electrocatalytic sites for SC applications. The XPS spectrum of C 1s corresponds to the following carbon bonds: 284.2 eV (C=C), 285 eV (C−N), 286.6 eV (C−O), and 288.2 eV (COOH) (Fig. S16f).[3]

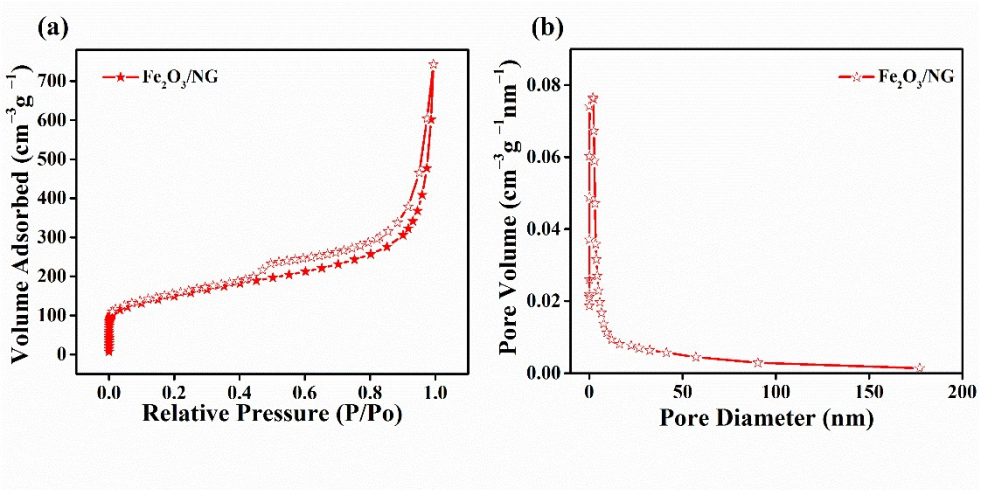


**Fig. S17** (a) $N_2$ sorption isotherms and (b) pore size distribution of the $Fe_2O_3$/NG aerogel.

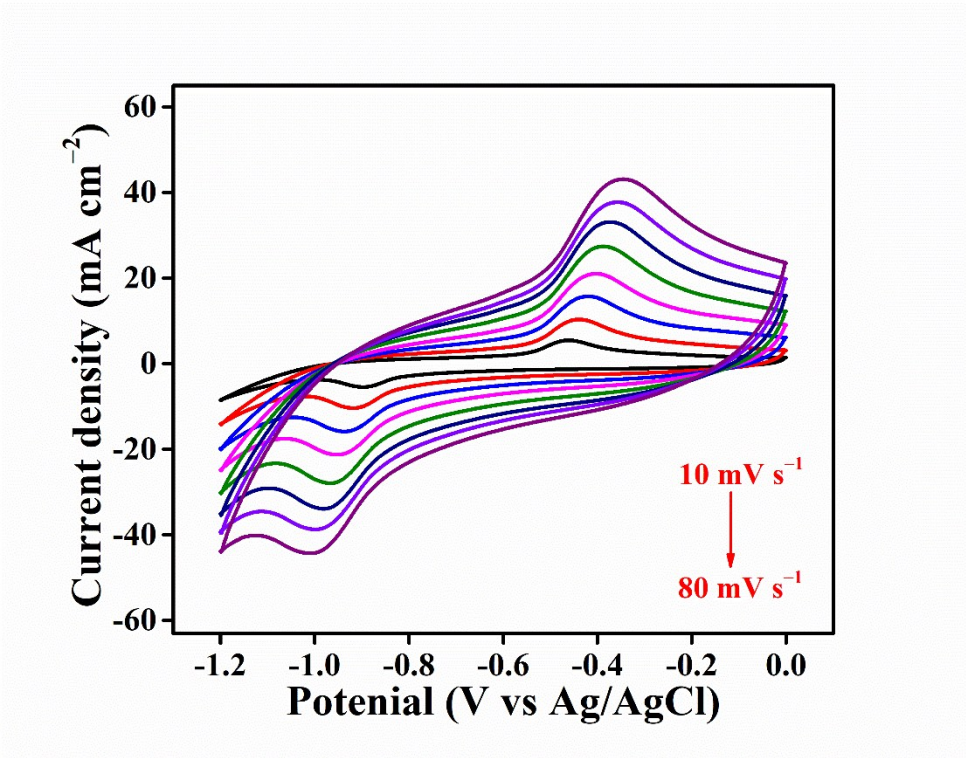


**Fig. S18** CV curves of $Fe_2O_3$/NG electrode at different scan rates from 10 to 80 mV $s^{-1}$.

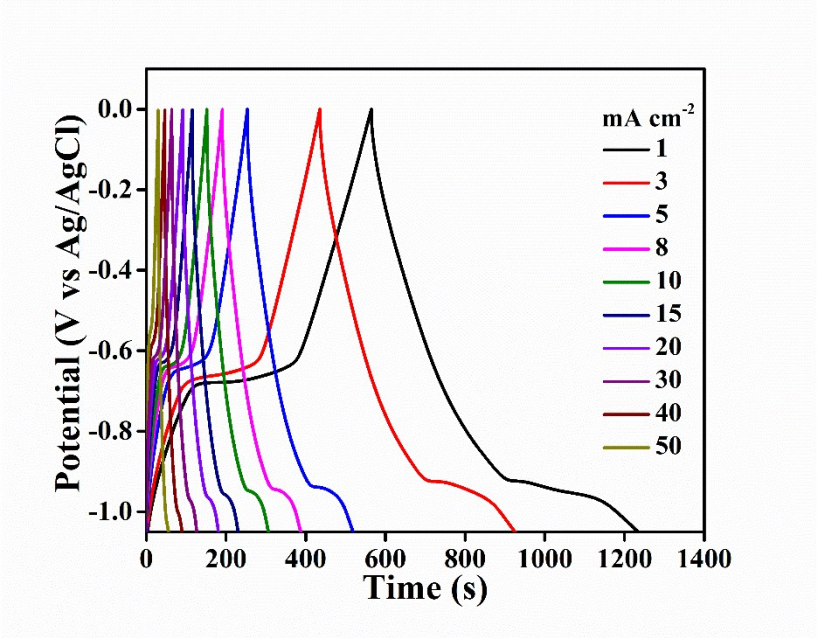


**Fig. S19** GCD curves of $Fe_2O_3$/NG electrode at different current densities from 1 to 50 mA $cm^{-2}$.

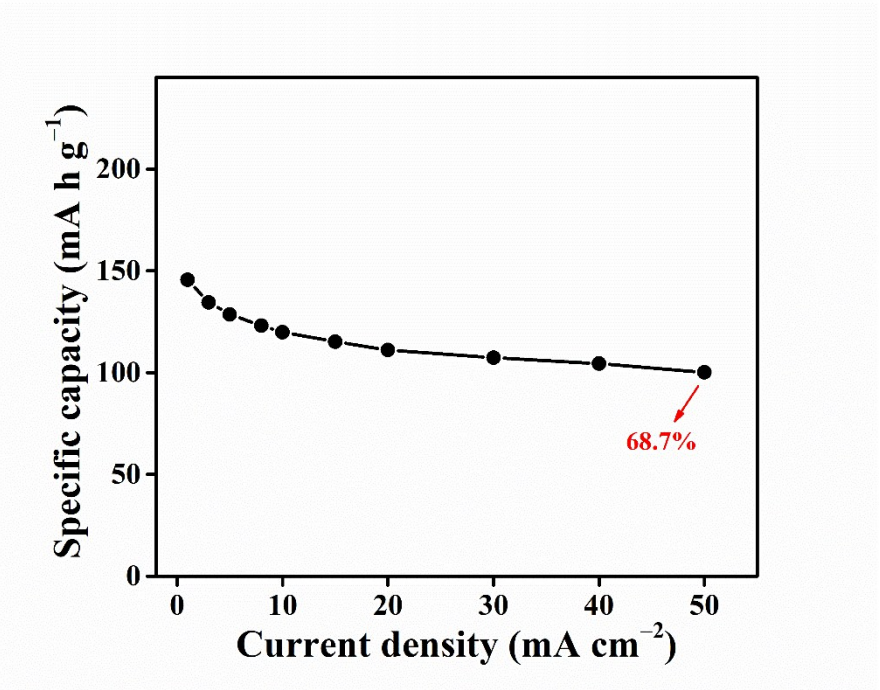


**Fig. S20** Specific capacity of $Fe_2O_3$/NG electrode as a function of current density.

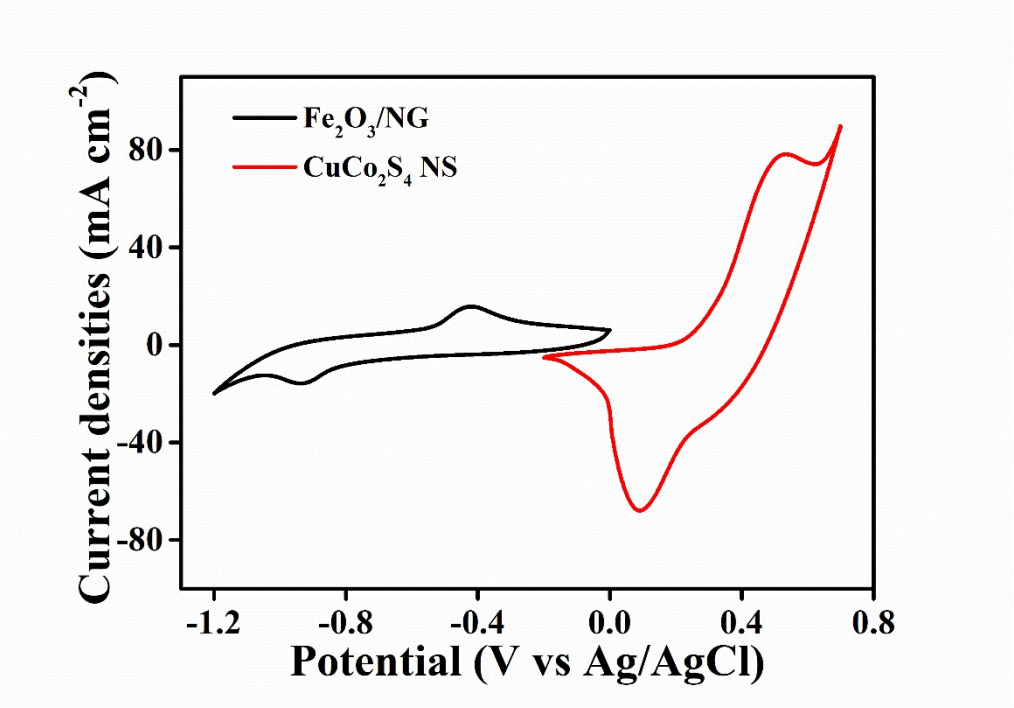


**Fig. S21** $Fe_2O_3$/NG (negative) and $CuCo_2S_4$ (positive) electrodes measured at a scan rate of 30 mV $s^{-1}$ in three-electrode configurations.

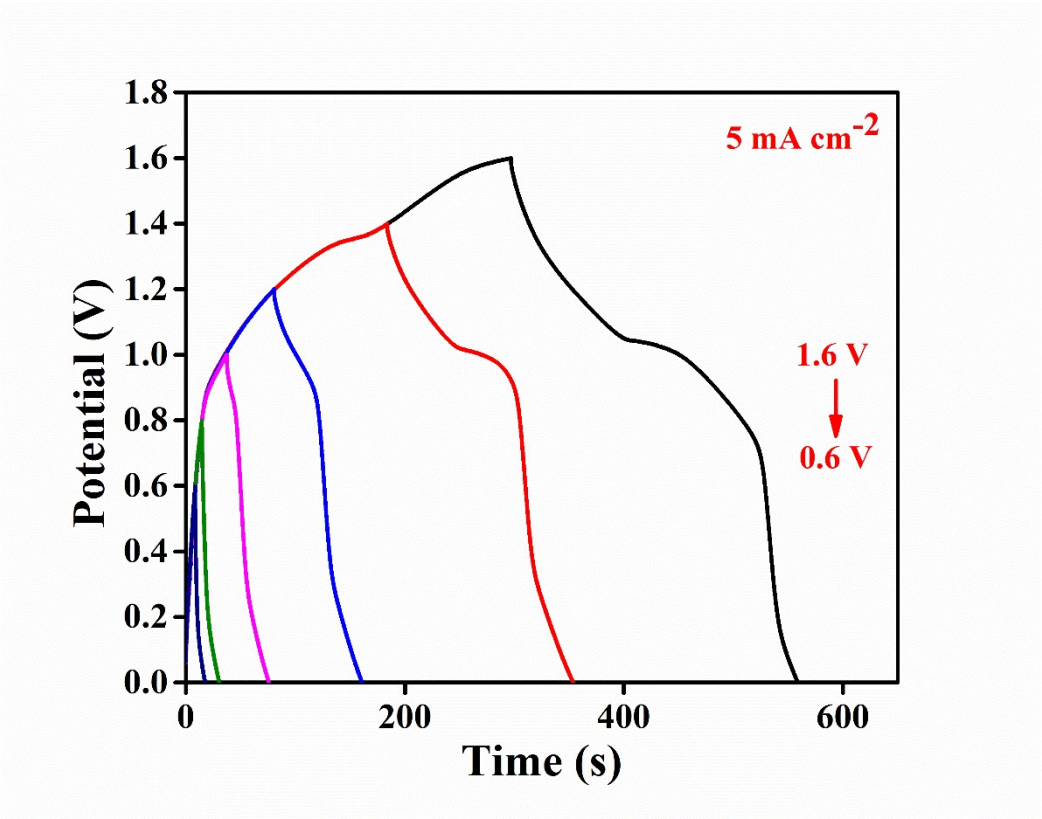


**Fig. S22** GCD of $CuCo_2S_4$//$Fe_2O_3$/NG ASC device at different potential windows from 0.6 to 1.6 V.

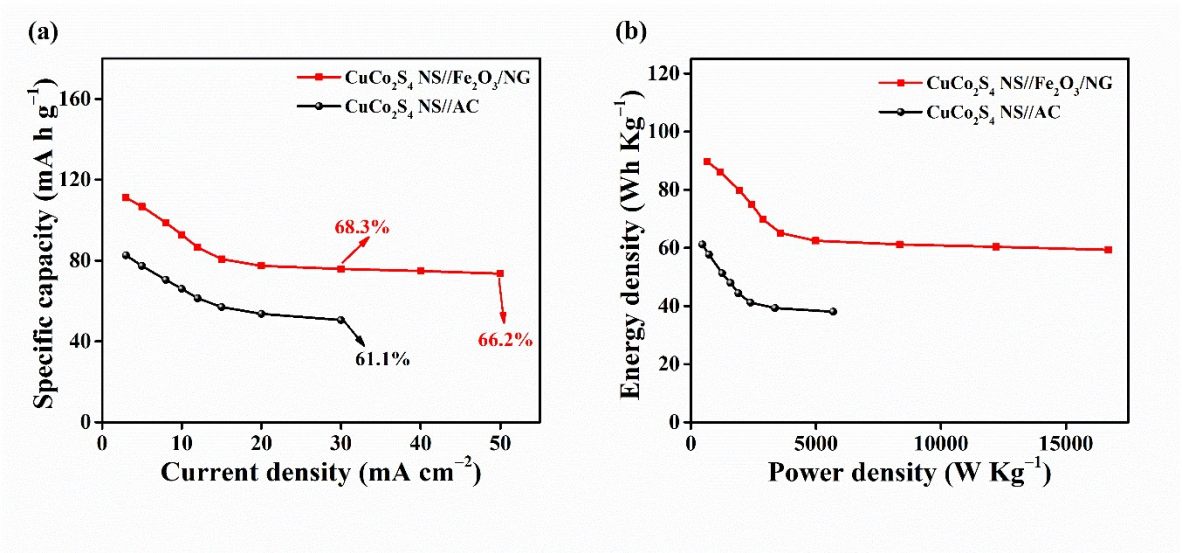


**Fig. S23** (a) specific capacities of the assembled devices as a function of current density, and (b) Energy vs power densities of the assembled $CuCo_2S_4$ NS//$Fe_2O_3$/NG and $CuCo_2S_4$ NS//AC ASC devices.

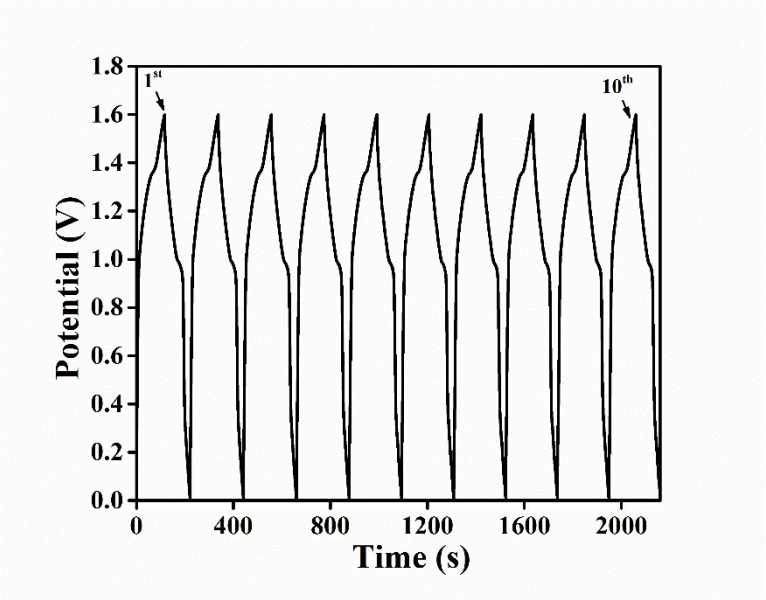


**Fig. S24** First 10 cycles of the $CuCo_2S_4$ NS//$Fe_2O_3$/NG ASC device at a current density of 30 mA $cm^{-2}$.

**Table S1** Elemental composition of $CuCo_2S_4$ NS and $Fe_2O_3$/NG estimated from XPS and ICP-OES.

| **Samples** | **Cu [at. %]** | **Co [at. %]** | **Fe [at. %]** | **C [at. %]** | **S [at. %]** | **N [at. %]** | **O [at. %]** |
|---|---|---|---|---|---|---|---|
| $CuCo_2S_4$ NS | 11.04 | 28.9 | – | – | 42.3 | – | 17.8 |
| $Fe_2O_3$/NG | – | – | 0.75 | 81.64 | – | 4.94 | 12.66 |

Cu, Co, S, Fe, N, C, and O contents were detected by XPS analysis and ICP-OES measurements

**Table S2** MOF derived $CuCo_2S_4$ NS electrode electrochemical properties comparison with reported literatures.

| **Electrode material** | **Areal capacitance/ capacity [F $cm^{-2}$/mA h $cm^{-2}$]** | **Specific capacitance/ capacity [F $g^{-1}$/mA h $g^{-1}$]** | **Current load** | **Electrolyte** | **Stability [Cycles]** | **References** |
|---|---|---|---|---|---|---|
| $CuCo_2S_4$ hollow nanoneedle arrays | - | 2163 F $g^{-1}$ | 6 mA $cm^{-2}$ | 0.6 M KOH | 96.3% [3000] | [4] |
| flower-like $CuCo_2S_4$ | - | 908.9 F $g^{-1}$ | 5 mA $cm^{-2}$ | 2 M KOH | 91.1% [2000] | [5] |
| Zn-Co-S NWs | 0.90 mAh $cm^{-2}$ | 366.7 mAh $g^{-1}$ | 3 mA $cm^{-2}$ | 6 M KOH | 93.2% [10000] | [6] |
| $FeCo_2S_4$-$NiCo_2S_4$ | 3.5 F $cm^{-2}$ | 1519 F $g^{-1}$ | 5 mA $cm^{-2}$ (2.2 A $g^{-1}$) | 3 M KOH | 77% [3000] | [7] |
| $NiCo_2S_4$@Ni-Mn-LDH | 1.74 F $cm^{-2}$ | - | 1 mA $cm^{-2}$ | 6 M KOH | 88.3% [1000] | [8] |
| Grass-like $Ni_3S_2$ nanorod/nanowire | 4.52 F $cm^{-2}$ | - | 1.25 mA $cm^{-2}$ | 3 M KOH | 108.3% [2000] | [9] |
| $NiCo_2S_4$ burl-like nanostructures | 1.19 F $cm^{-2}$ | - | 1 mA $cm^{-2}$ | 2 M KOH | 79.9% [2000] | [10] |
| $FeCo_2S_4$ | - | 2411 F $g^{-1}$ | 2 mA $cm^{-2}$ | 3 M KOH | 72% [5000] | [11] |
| $NiCo_2S_4$@$CoS_x$ core-shell | 4.74 F $cm^{-2}$ | - | 5 mA $cm^{-2}$ | 1 M KOH | 76.1% [1500] | [12] |
| $NiCo_2S_4$ nanotube arrays | 0.87 F $cm^{-2}$ | - | 4 mA $cm^{-2}$ | 1 M KOH | 96% [2000] | [13] |
| MOF derived $CuCo_2S_4$ NS arrays | 0.96 mAh $cm^{-2}$ | 409.2 mA h $g^{-1}$ | 3 mA $cm^{-2}$ (0.97 A $g^{-1}$) | 2 M KOH | 94.2% [10000] | This work |

**Table S3** ASCs device properties comparison with reported literatures.

| Reported ASC Device | Gravimetric/Geometric Capacity/Capacitance | Device Window [V] | Gravimetric/ Geometric Energy | Gravimetric/ Geometric Power | Electrolyte | Stability [Cycles] | References |
|---|---|---|---|---|---|---|---|
| Co-MOF/NF//AC | 4.84 F $cm^{-2}$ | 0-1.6 | 1.72 Wh $cm^{-2}$ | 4 W $cm^{-2}$ | 2 M KOH | 69.7% [2000] | [14] |
| Zn–Ni–P NS//$Fe_2O_3$@NG | 112.7 mAh $g^{-1}$ (1.99 mAh $cm^{-3}$) | 0-1.6 | 91.12 Wh $kg^{-1}$ | 611 W $kg^{-1}$ | PVA/KOH | 93 % [10000] | [15] |
| $CuCo_2S_4$//$MoO_2$@NC | 184 F $g^{-1}$ | 0-1.6 | 65.1 Wh $kg^{-1}$ | 800 W $kg^{-1}$ | PVA/KOH | 90.6% [5000] | [16] |
| Ni–Zn–Co–S-0.33 NSAs/NF//$Bi_2O_3$/NF | 114.7 mAh $g^{-1}$ (0.6 mAh $cm^{-2}$) | 0-1.6 | 91.7 Wh $kg^{-1}$ | 458 W $kg^{-1}$ | 3 M KOH | 88% [1000] | [17] |
| Ni-dMXNC//$Ti_3C_2T_x$ | 4.7 mAh $g^{-1}$ | 0-1.8 | 0.01 Wh $cm^{-3}$ | 0.22 W $cm^{-3}$ | 1 M KOH | 72.1% [5000] | [18] |
| $NiCo_2S_4$@$Ni(OH)_2$//AC | 159 F $g^{-1}$ | 0-1.8 | 65.7 Wh $kg^{-1}$ | 825 W $kg^{-1}$ | PVA/KOH | 90.7% [10000] | [19] |
| V-MOF//AC | 146.5 mF $cm^{-2}$ | 0-1.6 | 0.007 Wh $cm^{-3}$ | 0.07 W $cm^{-3}$ | PVA/ $Na_2SO_4$ | 93.6% [10000] | [20] |
| $NiCo_2S_4$//rGO | 111.5 F $g^{-1}$ | 0-1.5 | 38.6 Wh $kg^{-1}$ | 1330 W $kg^{-1}$ | PVA/KOH | 99.3% [5000] | [21] |
| $FeCo_2S_4$//3D PNG | - | 0-1.6 | 76.1 Wh $kg^{-1}$ | 755 W $kg^{-1}$ | PVA/KOH | 82% [10000] | [11] |
| $MnCo_2O_4$@CoS//AC | 151.8 F $g^{-1}$ | 0-1.6 | 55.1 Wh $kg^{-1}$ | 477.3 W $kg^{-1}$ | PVA/KOH | 91% [6000] | [22] |
| MOF derived $CuCo_2S_4$ NS arrays//$Fe_2O_3$/NG | 111.13 mAh $g^{-1}$ (2.1 mAh $cm^{-3}$) | 0-1.6 | 89.6 Wh $kg^{-1}$ 0.68 Wh $cm^{-3}$ | 663 W $g^{-1}$ (5.0 W $cm^{-3}$) | PVA/KOH | 91.5% [10000] | This work |

## References


1. T. Yamashita and P. Hayes, *Applied surface science*, 2008, **254**, 2441-2449.
2. L. Tang, Z. Xie, G. Zeng, H. Dong, C. Fan, Y. Zhou, J. Wang, Y. Deng, J. Wang and X. Wei, *RSC Adv*, 2016, **6**, 25724-25732.
3. M. Du, J. Sun, J. Chang, F. Yang, L. Shi and L. Gao, *RSC Adv*, 2014, **4**, 42412-42417.
4. S. E. Moosavifard, S. Fani and M. Rahmanian, *Chem Commun*, 2016, **52**, 4517-4520.
5. Y. Zhang, J. Xu, Y. Zhang, Y. Zheng, X. Hu and Z. Liu, *J Mater Sci*, 2017, **52**, 9531-9538.
6. C. Li, J. Balamurugan, N. H. Kim and J. H. Lee, *Adv energy Mater*, 2018, **8**, 1702014-1702026.
7. J. Zhu, S. Tang, J. Wu, X. Shi, B. Zhu and X. Meng, *Adv energy Mater*, 2017, **7**, 1601234.
8. H. Wan, J. Liu, Y. Ruan, L. Lv, L. Peng, X. Ji, L. Miao and J. Jiang, *ACS applied materials & interfaces*, 2015, **7**, 15840-15847.
9. T. Li, Y. Zuo, X. Lei, N. Li, J. Liu and H. Han, *J Mater Chem A*, 2016, **4**, 8029-8040.
10. M. Sun, J. Tie, G. Cheng, T. Lin, S. Peng, F. Deng, F. Ye and L. Yu, *J Mater Chem A*, 2015, **3**, 1730-1736.
11. S. Tang, B. Zhu, X. Shi, J. Wu and X. Meng, *Adv energy Mater*, 2017, **7**, 1601985.
12. W. Fu, C. Zhao, W. Han, Y. Liu, H. Zhao, Y. Ma and E. Xie, *J Mater Chem A*, 2015, **3**, 10492-10497.
13. H. Li, M. Yu, F. Wang, P. Liu, Y. Liang, J. Xiao, C. Wang, Y. Tong and G. Yang, *Nat Commun*, 2013, **4**, 1894.
14. G. Zhu, H. Wen, M. Ma, W. Wang, L. Yang, L. Wang, X. Shi, X. Cheng, X. Sun and Y. Yao, *Chem Commun*, 2018, **54**, 10499-10502.
15. T. T. Nguyen, J. Balamurugan, N. H. Kim and J. H. Lee, *J Mater Chem A*, 2018, **6**, 8669-8681.
16. S. Liu, Y. Yin, K. S. Hui, K. N. Hui, S. C. Lee and S. C. Jun, *Adv Sci*, 2018, **5**, 1800733-1800744.
17. Y. Huang, L. Quan, T. Liu, Q. Chen, D. Cai and H. Zhan, *Nanoscale*, 2018, **10**, 14171-14181.
18. Q. X. Xia, J. Fu, J. M. Yun, R. S. Mane and K. H. Kim, *RSC Adv*, 2017, **7**, 11000-11011.
19. J. Huang, J. Wei, Y. Xiao, Y. Xu, Y. Xiao, Y. Wang, L. Tan, K. Yuan and Y. Chen, *ACS Nano*, 2018, **12**, 3030-3042.
20. Y. Yan, Y. Luo, J. Ma, B. Li, H. Xue and H. Pang, *Small*, 2018, **14**, 1801815.
21. F. Lu, M. Zhou, W. Li, Q. Weng, C. Li, Y. Xue, X. Jiang, X. Zeng, Y. Bando and D. Golberg, *Nano Energy*, 2016, **26**, 313-323.
22. G. Liu, B. Wang, T. Liu, L. Wang, H. Luo, T. Gao, F. Wang, A. Liu and D. Wang, *J Mater Chem A*, 2018, **6**, 1822-1831.